Chapter 4

Surface Ribbon Method

For high-speed digital circuits the frequency spectrum spans from DC to high frequency where the skin and proximity effects occur, and for monolithic microwave integrated circuits (MMIC) the dimensions of the structures are shrinking. A unified methodology for evaluating parameters of interconnects and packages for wide range of frequencies would be desirable. Where the cross-sectional dimensions of structures reside within the wavelength of the highest significant frequency in the driving signal, the quasi-TEM approximation of the signal propagation should be valid. There have been many techniques developed for evaluating frequency-dependent resistance and inductance such as the finite element method (FEM) [49, 50], the boundary element method (BEM) [25, 51], the integral equation method (IEM) and the spectral domain method (SDM) [36, 52-58], etc.

As shown in previous chapters, the effective internal impedance (EII) approach can significantly reduce the computational load, but the EII approach should be appropriately incorporated with the field solvers. Recently, EII has been combined with the current integral equation [21, 22], and it has successfully been applied to calculating the conductor loss for twin and coplanar conductors. This technique is called the surface ribbon method (SRM) because it requires discretization only on the conductor surface instead of across the conductor cross-section, as in the volume filament method (VFM) [24], where the EII is used to represent resistance and internal inductance of the conductor. In this chapter, the accuracy of the SRM will be examined through various examples, such as single and twin conductors, a microstrip line, and

asymmetric striplines, and SRM will be explained from an electromagnetic point of view compared to the surface equivalent theorem. The SRM will be compared to previous work using standard impedance boundary conditions (SIBC) in conjunction with the integral equation method (IEM), or the spectral domain method (SDM). In addition, minimal discretization and accuracy will be examined, and for an example circuit the signal degradation and crosstalk will be evaluated to see the impacts of the skin and proximity effects on coupled lossy transmission lines.

4.1 Integral Equation Method using Standard Impedance Boundary Conditions and Volume Filament Method

There are various rigorous numerical techniques for characterizing lossy transmission lines, which are based on either the quasi-static assumption or a full-wave description. The FEM [49, 50] needs discretization of the entire domain to calculate electric and magnetic fields inside as well as outside of the conductor. To accurately calculate the fields, the size of the discretization should be sufficiently smaller than the wavelength inside of the conductor. And FEM is not so versatile for handling open boundary problems without approximations or the help of other techniques [49]. As shown in Chapter Two, BEM [25, 51] can be used without the limits of FEM, but it still requires considerable time in forming a matrix to be solved and it becomes inaccurate for inductance calculation at low frequency. The full-wave SDM [36, 52] or IEM can be utilized for characterizing the lossy transmission lines, but those are numerically expensive and complicated due to dyadic Green's functions for layered structures. Under the quasi-static assumption, the VFM [24] avoids the need of discretization outside of the conductor and complicated Green's functions, but it still needs fine discretization inside of the conductor as in FEM, and, therefore, it becomes

numerically intensive at high frequencies. In this sections, previous work on IEM and SDM are briefly reviewed which exploits modified SIBC or complicated dyadic Green's functions, and the classical technique of VFM is also summarized, from which SRM stems.

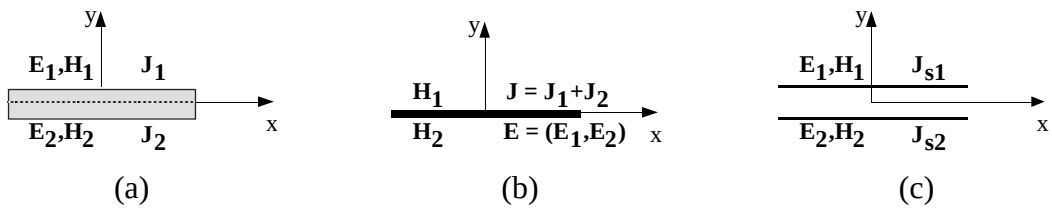

Figure 4.1: Modeling a lossy thick rectangular conductor in the integral equation method (IEM). (a) configuration of a thick rectangular conductor, (b) equivalent one thin plate with the surface impedance of a flat conductor, (c) equivalent two thin plates with the transfer impedance boundary condition.

4.1.1 Integral Equation Method and Spectral Domain Method

The integral equation method (IEM) and the spectral domain method (SDM) have been widely used to evaluate the propagation constant for various transmission lines at high frequency, where the latter transforms integral equations defined on the surface of the conductors into the spectral domain through Fourier transformations. As the finite thickness and finite conductivity of the conductor become important and the conductor loss is more significant the conventional IEM and SDM have been modified to evaluate the attenuation constant as well as the propagation constant. In reference [36, 52] the full-wave SDM was developed by deriving complicated dyadic Green's functions for planar stratified media where the lossy conductors are embedded. This approach is rigorous in that it faithfully describes the complex propagation

constant at low frequency as well as at high frequency, and it does not need a simplified model for the conductor geometries, and, therefore, takes care of edges as well as finite thickness of the conductor.

As in references [53-58], the full-wave or quasi-static integral equation could be combined with SIBC either in the space domain or in the spectral domain. The SIBC is applied to the equivalent infinitesimally thin impedance surface which replaces the lossy, thick conductor strips [53]. Because modeling the surface impedance becomes complicated at low frequency, SDM or IEM should be altered to consider low frequency behavior by defining the equivalent electric and magnetic currents on the surface of the conductor or by modifying SIBC, as explained in [54]. In [55] the transfer impedance boundary condition or the impedance matrix (2.5) is defined on both top and bottom plates, equivalent thin strip replaces the thick strip of Fig. 4.1(a) as shown in Fig. 4.1(b), equivalent electric field is defined by the weighted average of the tangential electric field, and equivalent current is equated to sum of surface current on both top and bottom surfaces of the strip. And in [56] the transfer impedance boundary condition is used under the assumption of a quasi-TEM mode, and two thin plates equivalently replace the thick conductor as shown in Fig. 4.1(c) and one thin plate replace the thick ground. As further approximations, in [57, 58] the thick conductor strip is equivalently replaced by a thin strip at the bottom of the conductor and the single-valued surface impedance of a thin flat conductor (2.4) is used to evaluate the conductor loss as well as the propagation constant.

Full-wave SDM or IEM with complicated dyadic Green's functions gives accurate results for low frequency as well as high frequency, but it requires intensive numerical work and complicated integral equations. Full-wave or quasi-TEM SDM or

IEM with the modified SIBC reduces the numerical burden and gives reasonable results. But these do not accurately capture the complex propagation constant, especially when the thickness of the conductor becomes appreciable compared to the width of the conductor, because the conductor is simplified into single or two plates and the edges of the conductor are ignored.

4.1.2 Volume Filament Method

Several approaches using the volume current integral equations have been utilized to evaluate frequency dependent resistance and inductance of lossy transmission lines [24, 57-64]. These techniques use the current density inside of the conductor as the state variables under the magneto-quasi-static assumption [65], i.e., the displacement current is negligible. The magnetic vector potential $\vec{A}$ is related to the current density $\vec{J}$ by

$$\vec{A}(r) = \frac{\mu}{4\pi}\int_{V'} \frac{\vec{J}(r')}{|r-r'|} dv', \tag{4.1}$$

where V' is the inside of the conductor, the magnetic vector potential and the magnetic field are given by $\mu\vec{H} = \nabla \times \vec{A}$, and the Coulomb gauge, $\nabla \cdot \vec{A} = 0$, is used. From Faraday's induction law and in sinusoidal steady state, the electric field and the magnetic vector potential is written as

$$\vec{E} = -j\omega\vec{A} - \nabla\phi \tag{4.2}$$

where ϕ is the scalar potential. And from the Ohm's Law the current density and the electric field are related by

$$\vec{J} = \sigma\vec{E}. \tag{4.3}$$

And (4.2) yields the current integral equation inside the conductor through substituting variables by (4.1) and (4.3)

$$\frac{\vec{J}(r)}{\sigma} + \frac{j\omega\mu}{4\pi}\int_{V'} \frac{\vec{J}(r')}{|r-r'|} dv' = -\nabla\phi\,. \tag{4.4}$$

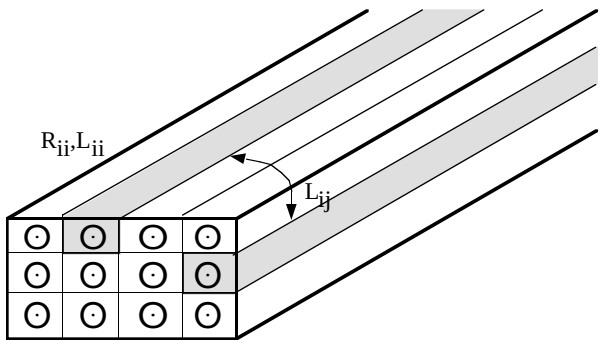

Figure 4.2: Discretization of the conductor inside for the use of the volume filament method (VFM). The conductor is segmented into small rectangular filaments, and the current on each filament is approximated with appropriate basis functions.

To account for the skin and proximity effects, which cause non-uniform current distribution inside of the conductor, the conductor is segmented into small elements, as shown in Fig. 4.2, and the current density is expanded by appropriate basis functions. Using the method of moments and pulse basis functions

$$\vec{J}(r) \cong \sum_{k=1}^{N} \frac{I_k}{a_k}\hat{i}_k, \tag{4.5}$$

where N is the total number of segments, I_k is the current of the filament k, a_k is the area of the filament k, and $\hat{i}_k$ is the unit vector of the current. The above equation is converted to

$$\left(\frac{l_m}{\sigma a_m}\right)I_m + \frac{j\omega\mu}{4\pi}\sum_{n=1}^{N}\left(\frac{1}{a_m a_n}\int_{V_m}\int_{V_n'}\frac{\hat{i}_m\cdot\hat{i}_n}{|r-r'|}dv'dv\right)I_n = \frac{1}{a_m}\int_{V_m}(\phi_1-\phi_2)dv, \quad (4.6)$$

where l_m is the length of the filament m, $\phi_1 - \phi_2$ is the potential difference applied between the ends of the filament m. The double integral of the above equation can be carried out using the closed form in [24] for infinitely long filaments or in [66] for finite length filaments in case of rectangular segmentation of the conductor. In matrix form, (4.6) becomes

$$([R] + j\omega[L])[I] = [V]. \quad (4.7)$$

And through appropriate matrix manipulation or solving, the series impedances of the multi-conductor lossy transmission lines are calculated.

This volume current integral equation approach is called Weeks' method, or the volume filament method (VFM). This approach can be formulated to handle obliquely placed multi-conductors as in [61] and afford three dimensional structure such as bend and ground plane as in [60], which is called the partial element equivalent circuits (PEEC) approach. As frequency goes up, the current crowds towards the surface and edges of the conductor. To accurately account for the profile of the current distribution, the size of the discretization should be sufficiently smaller than the skin depth. This makes the VFM numerically intensive at high frequencies. The computational load can be reduced by using adaptive meshing schemes as in [62, 64], cleverly developed iterative matrix solvers as in [64], or higher order of basis functions [63]. But the fine discretization is unavoidable at high frequency even though these approaches can save computation time. This problem can be overcome by

combining the current integral equation and the effective internal impedance (EII). The next section will deal with this recently proposed approach [21, 22].

4.2 Surface Ribbon Method

The volume current integral equation can be combined with the SIBC at high frequency like other numerical techniques such as BEM, FEM, SDM, etc. But at low frequency, higher order models for the surface impedance are required because the electric and magnetic fields do not locally relate to each other and the surface impedance at any point on the surface of the conductor becomes dependent on the global geometries of the conductors. But instead of using the Leontovich boundary condition, which relates external, tangential electric and magnetic fields at the conductor surface and removes the conductor interior from the domain of problem, the conductor can be modeled as a thin impedance sheet at the conductor surface, the conductor interior replaced with the exterior material, and the conductor interior included in the domain of problem. The conductor interior is represented at this sheet using EII, which relates the tangential electric field and the equivalent surface current density. The current integral equation can avoid the discretization of the conductor interior and, therefore, reduce the computational load fundamentally.

$$E_z = Z_{eii} J_s, \tag{4.8}$$

where E_z is the electric field parallel to the current flowing direction z, Z_{eii} is the EII, and J_s is the equivalent surface current. This equivalent surface current J_s can be expressed by the tangential magnetic fields

$$J_s = H_t^+ - H_t^-, \tag{4.9}$$

where H_t^+ and H_t^- are the tangential magnetic field outside and inside of the conductor, respectively. As frequency goes up H_t^- is vanishing and Z_{eii} is approaching the surface impedance Z_s, and the relation of (4.8) starts to satisfy the Leontovich boundary condition.

Using the equivalent surface current on the surface of the conductor instead of volume current inside of the conductor and the condition of (4.8) instead of the Ohm's Law, the volume current integral equation is substituted by the equivalent surface current integral equation as

$$\vec{Z}_{eii}(r)\cdot\vec{J}_s(r)+\frac{j\omega\mu}{4\pi}\int_{S'}\frac{\vec{J}_s(r')}{|r-r'|}ds'=-\nabla\Phi. \tag{4.10}$$

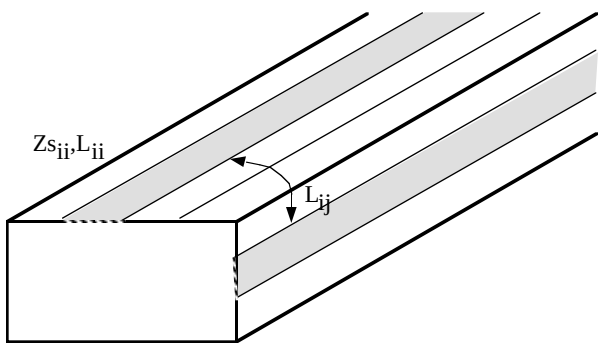

Figure 4.3: Discretization of the conductor surface for the use of the surface ribbon method (SRM). The conductor surface is segmented into small ribbons, the effective internal impedance (EII) is assigned at each ribbon, and the current on each ribbon is approximated with appropriate basis functions.

And as in VFM, the non-uniform surface current density at each segment, as shown in Fig. 4.3, on the conductor surface can be expanded using appropriate basis

functions. The pulse basis function can be used to represent the surface current density at each ribbon as follows

$$\vec{J}_s(r) \cong \sum_{k=1}^{N} \frac{I_k}{w_k} \hat{i}_k, \tag{4.11}$$

where w_k is the width of the filament k. By testing with the pulse basis function through the method of moments the surface current integral equation (4.10) gives following equation

$$\left(\tilde{Z}_{eii} \frac{l_m}{w_m}\right) I_m + \frac{j\omega\mu}{4\pi} \sum_{n=1}^{N} \left(\frac{1}{w_m w_n} \int_{S_m} \int_{S_n'} \frac{\hat{i}_m \cdot \hat{i}_n}{|r - r'|} ds' ds \right) I_n = \frac{1}{w_m} \int_{S_m} (\phi_1 - \phi_2) ds, \tag{4.12}$$

where $\tilde{Z}_{eii}$ is the weighted-averaged effective internal impedance, l_m is the length of the ribbon m, and I_m and I_n are the surface current on the ribbon m and n, respectively. The double surface integral can be easily calculated by using the simple logarithmic function in [27] for infinitely long ribbons or the logarithmic and inverse trigonometric function in [66] for a ribbon of finite length. The above equation can be represented by the following matrix form

$$\left(\left[\tilde{Z}_{eii}\right] + j\omega[L]\right)[I] = [V] \tag{4.13}$$

where the real term of EII represents resistance, and the imaginary term of EII and the second term are used to give inductance.

This surface current integral equation approach combined with EII is called the surface ribbon method (SRM). Unlike VFM, by using EII SRM gets rid of the conductor interior from the domain to be solved and, therefore, requires discretization only on the surface of the conductor. The following sub-sections will explain the

scheme of discretization, the weighted averaged effective internal impedance, and the electromagnetics of SRM compared to VFM and the surface equivalent theorem, respectively.

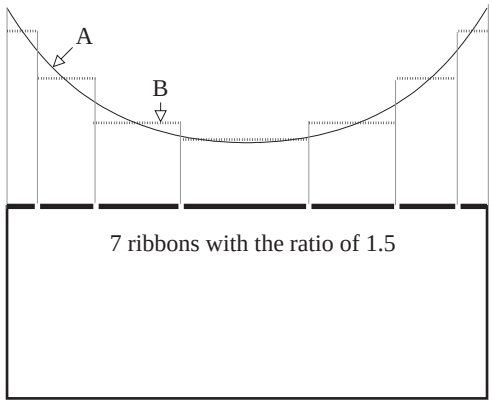

Figure 4.4: Non-uniform discretization and the weighted-averaged effective internal impedance. The conductor surface is sequentially divided into non-equal width segments with a certain width ratio and the weighted-averaged effective internal impedance (EII) is assigned at each ribbon. A(solid line): position-dependent effective internal impedance; B(dotted line): weighted-averaged effective internal impedance.

4.2.1 Discretization and Weighted-averaged Effective Internal Impedance

Since the SRM represents the conductor interior at the conductor surface, the current is defined only on the conductor surface. The surface current is mainly determined by the resistive term of EII at low frequency and by the skin and proximity effects at high frequency, and, therefore, it becomes non-uniform due to the position-dependent EII at low frequency and due to the current crowding towards the corners at high frequency. In order to properly capture the non-uniform surface current, discretization on the conductor surface is required, as shown in Fig. 4.3. To reduce the number of unknowns an adaptive meshing scheme can be used as in VFM [62, 64].

The conductor surface is sequentially divided into non-equal width segments with a certain ratio, shown in Fig. 4.4. In VFM a skin depth needs to be divided into several segments in order to capture the exponentially decreasing current profile. The surface current in SRM does not change as quickly as the current of the conductor interior in VFM. Thus, in SRM the smallest segment is chosen to be a skin depth or less depending on the highest frequency of interest, the number of segments, and the ratio between segments.

The surface current is expanded by the pulse basis function, (4.11), and a constant surface current is defined at each ribbon. By testing with the pulse basis function the surface current integral equation gives the matrix equation (4.12). In this process the position-dependent EII is also tested by the pulse basis function, and a singled-valued, weighted-averaged EII is defined at each ribbon, as shown in Fig. 4.4, thus producing a step-wise constant EII

4.2.2 Internal Inductance and External Inductance

From the Poynting theorem with the assumptions of non-radiation and quasi-static fields, the following equation is derived for the volume current integral equation

$$-\int_{V_c} \nabla\phi \cdot \vec{J}^* dv = \frac{1}{\sigma}\int_{V_c} \vec{J} \cdot \vec{J}^* \, dv + j\omega \int_{V_c} \vec{A} \cdot \vec{J}^* \, dv, \tag{4.14}$$

where V_c is the conductor interior, V_{out} is the conductor exterior, the left-hand side of the equation is the power applied, the first term of the right-hand side is the ohmic loss, and the second term corresponds to the inductance as

$$\int_{V_c} \vec{A} \cdot \vec{J}^* \, dv = \mu \int_{V_c} \vec{H} \cdot \vec{H}^* \, dv + \mu \int_{V_{out}} \vec{H} \cdot \vec{H}^* \, dv = \left(L_{\text{int}} + L_{ext}\right)|I|^2. \tag{4.15}$$

This can be decomposed into the internal inductance and the external inductance as

$$L_{\text{int}} = \frac{\mu}{|I|^2}\int_{V_c} \vec{H}\cdot\vec{H}^* dv = \frac{1}{|I|^2}\int_{V_c} \vec{A}\cdot\vec{J}^* dv - \frac{1}{|I|^2}\int_{S_c}\left(\vec{A}\times\vec{H}^*\right)\cdot\hat{n}ds \tag{4.16}$$

$$L_{ext} = \frac{\mu}{|I|^2}\int_{V_{out}} \vec{H}\cdot\vec{H}^* dv = \frac{1}{|I|^2}\int_{S_c}\left(\vec{A}\times\vec{H}^*\right)\cdot\hat{n}ds$$

where S_c is the conductor surface and $\hat{n}$ is outward normal unit vector on the conductor surface.

Also the Poynting theorem gives the following relationship for the surface current integral equation

$$-\int_{S_c}\nabla\phi\cdot\vec{J}^* ds = \int_{S_c} Z_{eii}\,\vec{J}\cdot\vec{J}^* ds + j\omega\int_{S_c}\vec{A}\cdot\vec{J}^* ds, \tag{4.17}$$

where S_c is the conductor surface. In the right-hand side of above equation, the ohmic loss is given by

$$R = \frac{1}{|I|^2}\int_{S_c}\text{Re}\{Z_{eii}\}\,\vec{J}\cdot\vec{J}^* ds \tag{4.18}$$

and the internal inductance and the external inductance are arranged as follows

$$L_{\text{int}} = \frac{1}{\omega|I|^2}\int_{S_c}\text{Im}\{Z_{eii}\}\,\vec{J}\cdot\vec{J}^* ds - \frac{1}{|I|^2}\int_{S_c}\left(\vec{A}\times\vec{H}^*{}_{in}\right)\cdot\hat{n}ds \tag{4.19}$$

$$L_{ext} = \frac{1}{|I|^2}\int_{S_c}\left(\vec{A}\times\vec{H}^*{}_{out}\right)\cdot\hat{n}ds,$$

where $\vec{H}^*{}_{in}$ and $\vec{H}^*{}_{out}$ are the magnetic field intensity inside and outside of the conductor surface, respectively. And the second term of L_{int} and L_{ext} are summed to correspond to the second term of the right-hand side of (4.17).

$$\frac{1}{|I|^2}\int_{S_c}\left[\vec{A}\times\left(\vec{H}^*{}_{out}-\vec{H}^*{}_{in}\right)\right]\cdot\hat{n}ds=\frac{1}{|I|^2}\int_{S_c}\vec{A}\cdot\vec{J}^*\,ds \tag{4.20}$$

Therefore, the real term of EII gives the resistance of the lossy transmission lines, the sum of the imaginary term of EII and the magnetic energy stored inside of the contour surrounded by ribbons corresponds to the internal inductance, and the magnetic energy stored outside of the conductor corresponds to the external inductance.

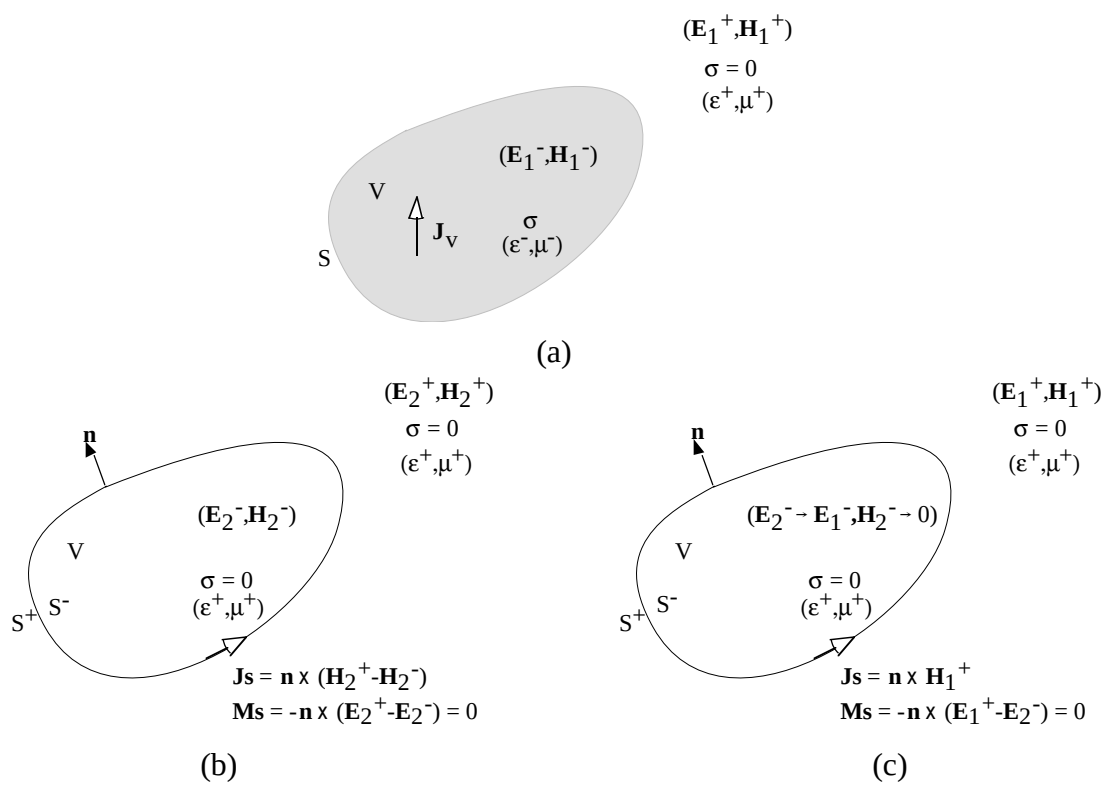

Figure 4.5: Comparison of the actual geometry and the equivalent model for the surface ribbon method (SRM). (a) Actual geometry with the descriptions of fields and material properties, (b) At low frequency equivalent model for the surface ribbon method (SRM) with the descriptions of fields and material properties, (c) At high frequency equivalent model for the surface ribbon method (SRM) with the descriptions of fields and material properties.

4.2.3 High and Low Frequency Behavior of Surface Ribbon Method

The conductor in Fig. 4.5(a) is modeled as the thin cylindrical shell shown in Fig. 4.5(b) and (c). At high frequency as shown in Fig. 4.5(c) the electric and magnetic fields outside of the conductor approach to those of original domain because the EII approaches the surface impedance, the magnetic field inside of the conductor starts to vanish, the relation between the electric and magnetic fields is localized, and, hence, the Leontovich boundary conditions begin to be satisfied. Therefore, SRM at high frequency just satisfies the surface equivalent theorem [67].

At low frequency, as shown in Fig. 4.5(b) the electric and magnetic fields are not the same as the original problem not only inside the conductor but also outside the conductor. Therefore, it does not satisfy the surface equivalent theorem. But at low frequency the current distribution is determined by the resistive term of the impedance. Hence, the series impedance of lossy transmission lines is calculated with appropriate definition of EII, which gives DC resistance and approximately yields the current distribution giving accurate internal and external inductance at low frequency and approaches to SIBC at high frequency. And as shown in Fig. 2.6, the modified plane wave model and the transmission line model for the EII give accurate internal and external inductances for a wide range of width to thickness ratio for rectangular conductors at low frequency.

4.2.4 Surface Ribbon Method vs. Integral Equation Method using Standard Impedance Boundary Condition

Under the quasi-static assumption, the integral equations using modified SIBC [56-58] are the same form as (4.17). Both exploit free space Green's function for non-

magnetic media and define the surface current on the conductor surface. The only difference is that IEM approximates the conductor strip as one or two plates and uses the impedance matrix or the surface impedance of the flat conductor as SIBC, while the SRM models the conductor as a thin cylindrical shell preserving the original shape and the single-valued EII all over the conductor surface. Therefore, SRM takes care of the edges and corners of the conductor, unlike IEM, and can give accurate results regardless of size and shape of the conductor.

4.3 Examples

Several examples have been considered to determine the accuracy and efficiency of SRM. At first, single and twin circular and rectangular conductors are examined. The modified plane wave model and the transmission line model for EII are compared and the better results are obtained using the transmission line model; the illustrated examples make use of the transmission line model unless otherwise noted. And, as shown in Chapter Three, the series impedance is calculated in the case of a V-shaped conductor-backed coplanar waveguide (VGCPW) and microstrip lines. Minimal segmentation is considered for asymmetric striplines, and previous work using the IEM combined with SIBC and SRM are compared for a microstrip line. To verify the accuracy of the results and efficiency, SRM is compared results of rigorous VFM [24] and BEM [25].

4.3.1 Single and Twin Circular Conductors

As shown in Fig. 4.6, resistance and inductance have been calculated by SRM and BEM, and compared with each other for a single circular conductor and twin circular conductors of 1mm radius, 0.2 mm gap, and conductivity 5.8×10^{7} [S/m]. For

the single circular conductor of Fig. 4.6(a), resistance and inductance from the SRM are almost identical to the results of BEM for all frequencies considered. For closely coupled parallel twin circular conductors, shown in Fig. 4.6(b), resistance and inductance of SRM match well to results of BEM at high and low frequencies within a 2% error, and at mid frequency the resistance and inductance are off 7% and 6%, respectively. For these examples the conductor is uniformly segmented with 90 segments.

4.3.2 Single and Twin Rectangular Conductors

As shown in Fig. 4.7, resistance and inductance have been calculated by SRM, VFM, and BEM, and compared with each other for a single rectangular conductor and twin rectangular conductors 20 μm wide, 4 μm thick, 4 μm gap, and conductivity 5.8×10^7 [S/m]. For single rectangular conductor of Fig. 4.7(a), resistance and inductance from the SRM using the transmission line model (TLM) for EII agree with the results of VFM and BEM within a deviation of 2% for resistance and 0.1% for inductance for all frequencies considered. The low frequency inductance calulated by SRM using the modified plane wave model (MPWM) deviates about 0.3% from the others. For closely coupled parallel twin rectangular conductors, shown in Fig. 4.7(b), resistance and inductance of SRM using TLM match well to results of VFM and BEM at high and low frequencies within 2%, and at mid frequency the resistance and inductance are off 10% and 6%, respectively. SRM using MPWM overestimates low frequency inductance by 3.5%. For closely coupled coplanar twin conductors, shown in Fig. 4.7(c), all calculated resistance and inductance values agree well with each other for all frequencies with less than 2% deviation, except SRM using MPWM underestimates the low frequency inductance by 4.5%. For these examples the conductor is non-uniformly segmented with 20 segments across the wide faces with

width ratio of 1.1, and 4 segments across the narrow face with width ratio of 2.

As shown in Fig. 3.6 and Fig. 3.8, SRM and VFM have been used to calculate the series impedance for various geometries of VGCPW and microstrip lines. For those examples, SRM gives the same results as VFM. And the gain in efficiency of SRM over VFM is shown in Table 3.1, where the number of unknowns is reduced to about one-thirds and computation time to at least one-twentieth for the same discretization scheme. Because SRM needs the discretization only on the conductor surface and the decay of current is less severe along the conductor surface than inward into the conductor, the number of segments can reduced more compared to the number of filaments on the conductor surface in VFM.

4.3.3 A Microstrip Line : Comparison of Surface Ribbon Method and Integral Equation Method

The series impedance of a microstrip line has been calculated by SRM and IEM using approximated SIBC [58], where the signal line is 10 μm wide, 5 μm thick, and 5 μm above a ground plane. In IEM the signal line is approximated as a thin plate at the bottom of the conductor and the surface impedance of a flat conductor is used as the SIBC. SRM uses ten segments (for the wide surface) and five segments (for the narrow surface) for the signal line and 50 segments for the ground plane with width ratios of 1.8, 3, and 0.85, respectively, VFM uses 10×5 segments for the signal line and 50×5 segments for the ground plane with width ratios of 1.8, 3, 0.85 and 3, respectively, and IEM uses 10 segments for the signal line and 50 segments for the ground with width ratios of 1.8 and 0.85, respectively. Also the minimal segmentation scheme in SRM is derived and Fig. 4.8 shows that scheme for a microstrip line

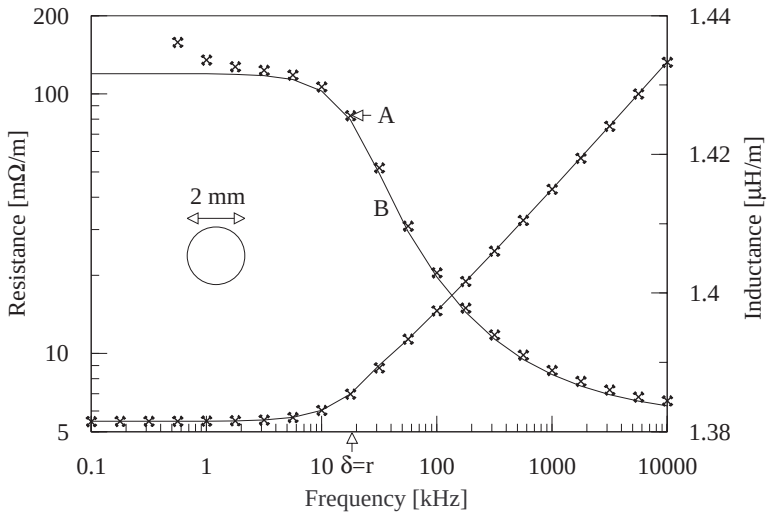

(a) For a circular conductor

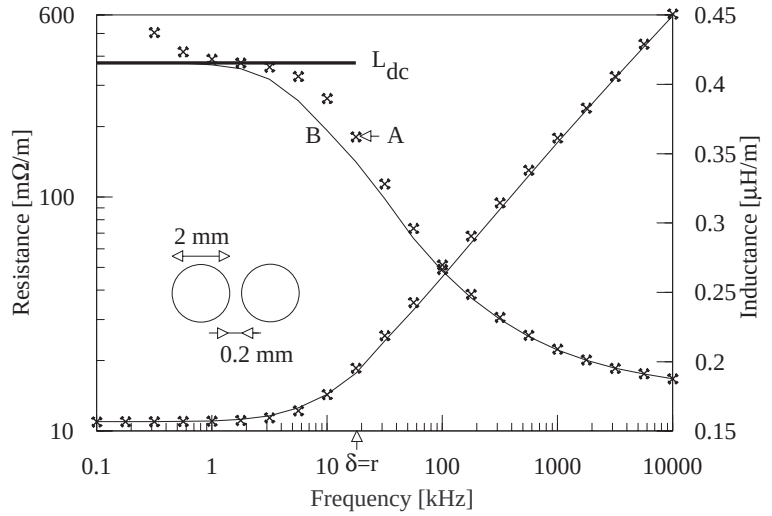

(b) For twin circular conductor

Figure 4.6: Comparison of resistance and inductance between surface ribbon method (SRM), and boundary element method (BEM). A(⋇): BEM; B(solid line): SRM.

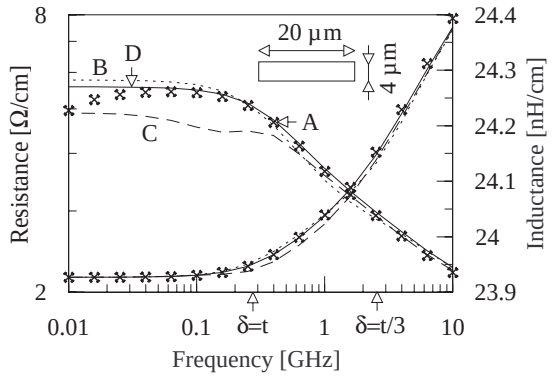

(a) For a rectangular conductor

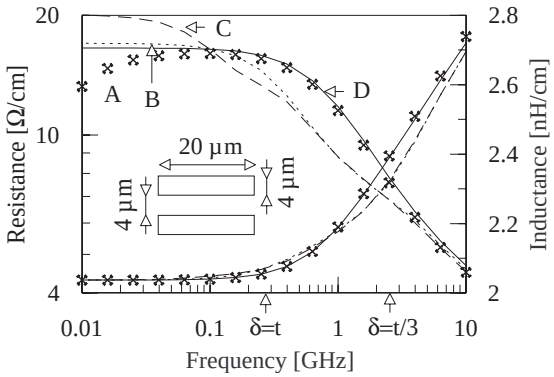

(b) For twin parallel rectangular conductors

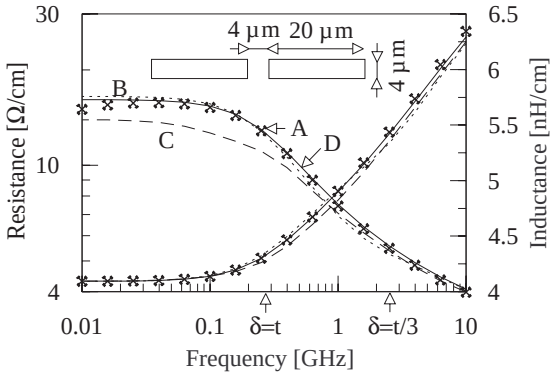

(c) For twin coplanar rectangular conductors

Figure 4.7: Comparison of resistance and inductance between volume filament method (VFM), surface ribbon method (SRM), and boundary element method (BEM). A(⨯): BEM; B(dotted line): SRM using transmission line model; C(dashed line): SRM using modified plane wave model; D(solid line): VFM.

structure, where one segment is assigned at each side of the conductor and the ground is divided into 5 segments, so the total number of segments are 9. Figure 4.9 compares the results of different methods used. SRM and VFM give well matched results but resistance and inductance of IEM are 27% and 23% off, respectively, from the results of SRM and VFM. In SRM the signal line is approximated into two plates, one on the top and one on the bottom surface for comparison, and the surface impedance of a flat conductor used as the EII. This is a similar approach as in previous work on the IEM, but previous work use the impedance matrix for the two plate approximation and simplify further. The results of this simplification gives resistance and inductance within 24% and 9% deviations from the results of SRM and VFM, respectively. SRM with the minimal segments gives better results than IEM and SRM with the two plate approximation. When the minimal segments of 9 is used in SRM, the resistance is off about 2% from the result of SRM using finer segments and the inductance is overestimated by 10% and 2.5% at low and high frequencies, respectively, compared to the results of SRM using finer segments. In Table 4.1 the number of unknowns and computation time for matrix assembling and solving are shown. SRM reduces the number of unknowns to less than one-third and computational time to almost one-thirtieth for the same discretization scheme and at minimal segments the number of unknowns is reduced to about one-thirtieth and computation time is decreased by almost three orders of magnitude with reasonable error. Because IEM approximates the thick conductor as one or two thin strips, it gives only approximate results, unlike SRM that calculates accurate resistance and inductance without modification of the geometries. The error caused by simplifying the geometries is decreasing as the ratio of conductor width to conductor thickness (w / t) and the ratio of dielectric height to

conductor thickness (h / t) are increasing, gets worse for closely coupled lines, and in this example the ratios are as 2 and 1, respectively, and the error is too large.

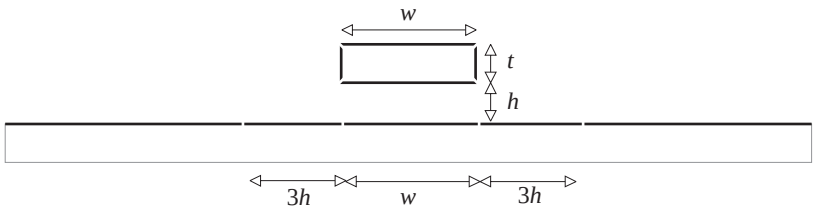

Figure 4.8: Minimal segmentation of a microstrip line. Signal line is segmented into 4 ribbons and the ground plane is divided into 5 ribbons, where the width of each ribbon is dependent only on the dimensions of the structure such as signal line width, thickness, and height above the ground.

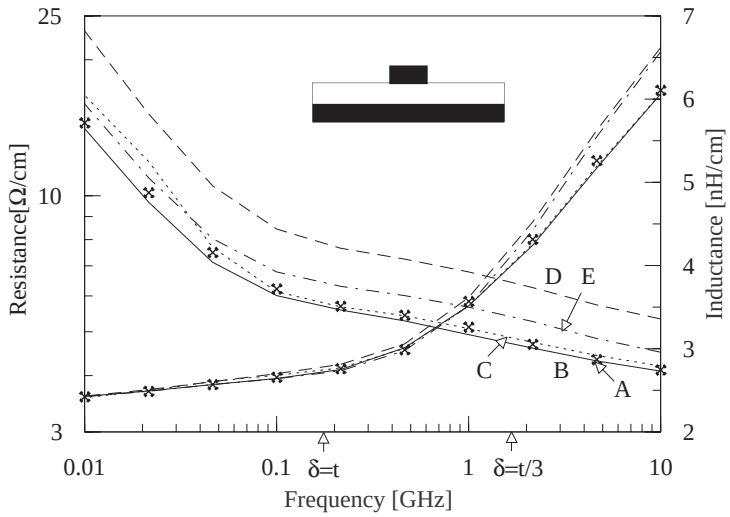

Figure 4.9: Comparison of resistance and inductance of a microstrip line between volume filament method (VFM), surface ribbon method (SRM), and integral equation method (IEM) using the modified standard impedance boundary condition (SIBC). A(⨯): VFM; B(solid line): SRM; C(dotted line): SRM with minimal segments; D(dashed line): IEM; E(dot-and-dashed line): SRM assuming two plates for the signal line.

Method	Number of unknowns	CPU time[sec] Assembling	Solving per freqeun
VFM	300	9.63	9.64
SRM α	80	0.60	0.29
SRM$^{\beta}$	9	*	0.01
IEM	60	0.22	0.10
SRM$^{\gamma}$	70	0.51	0.14

Table 4.1: Comparison of run times on an IBM RISC 6000 for volume filament method (VFM), surface ribbon method (SRM), and integral equation method. SRM and VFM use gaussian elimination as a matrix solver, α uses fine segments, β uses minimal segments, γ assumes two plates for the signal line, and * is negligible time.

For comparison, two other minimum segmentation schemes in SRM are also considered. Firstly, a single segment has been assigned to the ground plane. Secondly, the ground plane is discretized into three segments: one segment directly below the signal line with the width of w , and one more segment on each side for the remaining ground plane. Both use four segments for the signal line. For two different microstrip line geometries, resistance and inductance have been calculated using the different segmentation schemes of SRM, as well as with full VFM and a finely divided SRM; example 1 has a signal line 10 µm wide (w = 10 µm) and 10 µm thick (t = 10 µm), and a ground plane 500 µm wide and 10 µm thick, where VFM uses 10×10 segments for the signal line and 80×7 segments for the ground plane with width ratios of 1.57, 1.57, 0.89, and 2.7, respectively. Example 2 has a signal line of 10 µm wide and 1 µm thick, and a ground plane 500 µm wide and 1 µm thick, where VFM uses 14×6 segments for the signal line and 80×6 segments for the ground plane with width ratios of 2.06, 3.2, 0.89, and 3.2, respectively. For both examples SRM with fine segments uses the same segmentation scheme of VFM except the ground plane is

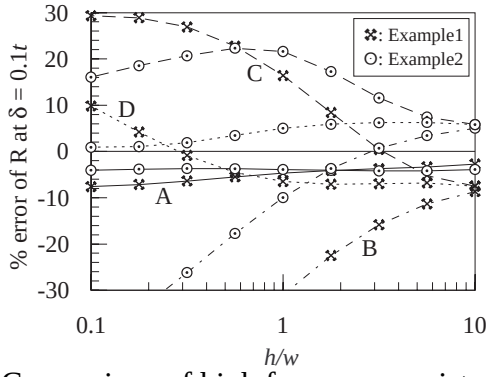

(a) Comparison of high frequency resistance

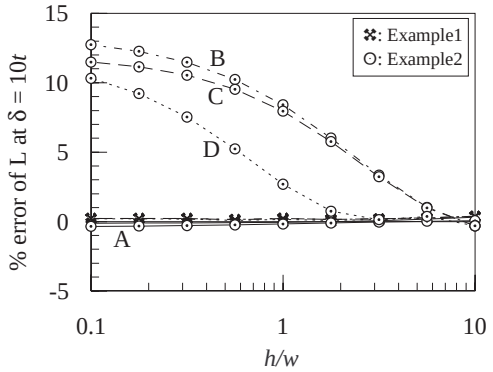

(b) Comparison of low frequency inductance

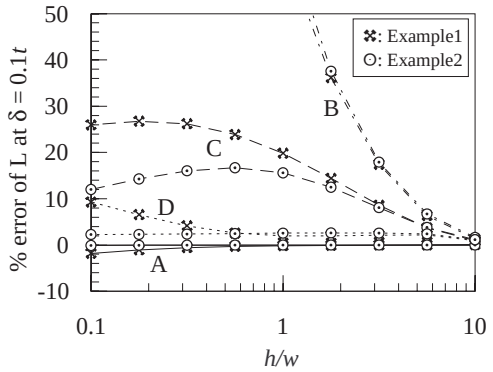

(c) Comparison of high frequency inductance

Figure 4.10: Comparison of resistance and inductance calculated using different segmentations in SRM. Resistance and inductance are normalized by the results of VFM. A(solid line): fine segments; B(dot-and-dashed line): one segment for the ground plane; C(dashed line): three segments for the ground plane; D(dotted line): five segments for the ground plane. Minimum segmentations use four segments for the signal line.

segmented into one layer at the top surface. Figure 4.10 compares resistance and inductance as a function of strip height above the ground plane h, from $0.1\times w$ to $10\times w$ at the low frequency where $\delta = 10t$, and the high frequency where $\delta = 0.1t$. With five segments for the ground plane SRM gives accuracy within 10% for resistance and inductance for both examples. With three segments for the ground SRM deviates by as much as 30% for resistance and inductance.

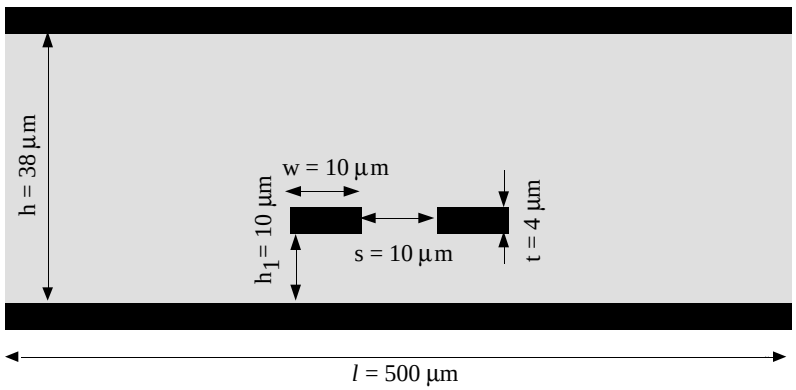

Figure 4.11: 50 Ω coupled asymmetric striplines. The signal lines are 10 µm wide, 4 µm thick, 10 µm gap over a bottom ground plane and between signal lines, conductivity 5.8×10^7 [S/m], and 38 µm thick dielectric.

4.3.4 Asymmetric Coupled Striplines

Another example to verify accuracy and efficiency of SRM are the asymmetric coupled striplines shown in Fig. 4.11, which could be an interconnect structure of a multichip module (MCM). The signal lines are 10 µm wide, 4 µm thick, 10 µm gap over a bottom ground plane and between signal lines, metal conductivity 5.8×10^7 [S/m], and 38 µm thick dielectric. In SRM the signal line is segmented by 10 and 4 segments for each side with width ratios of 1.4 and 2, respectively, and the ground is divided into 50 segments with width ratio of 0.85. VFM uses the same segmentation scheme as in SRM and the ground is segmented into 50×4 filaments. Also the mini-

mal segmentation scheme is used in SRM, and in this case the total number of segments is 9. For all frequencies, in Fig. 4.12, SRM gives the results close to VFM within 2% deviation. When the minimal segments of 22 is used in SRM, resistance and inductance are compared to those with finer segments at low, mid, and high frequencies, respectively, as follows; R_{11} is off about 0.5%, 5%, and 2%, R_{12} is off about 8%, 16%, and 10%, L_{11} is off about 1.5%, 0.5%, and 2%, and L_{12} is off about 4%, 5%, and 3%. In Table 4.2 the number of unknowns and computation time for matrix assembling and solving are shown. SRM reduces the number of unknowns to less than one-third and computational time to almost one-thirtieth for the same discretization scheme and at minimal segments the number of unknowns is reduced to about one-twentieth and computation time is decreased by almost three orders of magnitude with reasonable error.

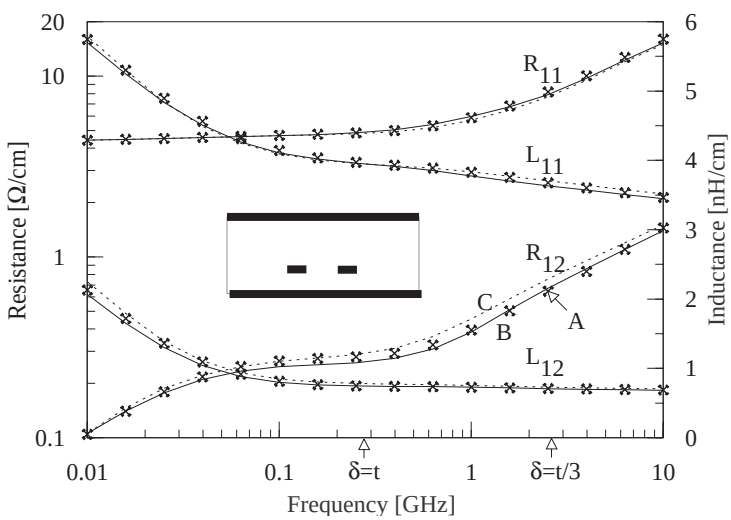

Figure 4.12: Comparison of resistance and inductance of coupled asymmetric striplines between volume filament method (VFM), surface ribbon method (SRM) with the same segmentation scheme as VFM, and surface ribbon method (SRM) with minimal segments. A(⤫): VFM; B(solid line): SRM; C(dotted line): SRM with minimal segments.

Method	Number of unknowns	CPU time[sec] Assembling	Solving per freqeuncy
VFM	480	25.6	39
SRM	156	2.1	1.7
SRM*	22	**	0.043

Table 4.2: Comparison of run times on an IBM RISC 6000 for volume filament method (VFM) and surface ribbon method (SRM). SRM and VFM use gaussian elimination as a matrix solver, * uses minimal segments, and ** is negligible time.

4.3.5 Crosstalk on Lossy Transmission Lines

As an example showing the skin and proximity effects on signal degradation and crosstalk, asymmetric coupled striplines, shown in Fig. 4.11, with varying length and termination, have been analyzed using the fast Fourier transform (FFT). The thin film conductors are assumed to be embedded in a lossless homogeneous dielectric medium of dielectric constant 3.5, and, therefore, the capacitance matrix $[C]$ is obtained from the inverse of the matrix $[L_{ext}]$. Figure 4.13 shows the circuit to be analyzed, where the load capacitance C_{L1} and C_{L2} are 0.1 pF, and the resistances of the series terminations (R_{S1}, R_{S2}) are 9 Ω or 50 Ω (i.e., unmatched or matched to the high frequency characteristic impedance of striplines).

As an input signal, a trapezoidal pulse is assumed with 0.1 ns rise and fall time and the pulse width T_w of 0.3 ns. Figure 4.14 shows the spectrum of the input pulse. The effective bandwidth is calculated as 2.26 GHz, at which frequency the skin depth is almost one-third of the conductor thickness. Figure 4.15(a) and (b) show the signal on the active line and far-end crosstalk of the quiet line, when the length of line is 15 cm and matched termination is used. For comparison voltage profiles are also obtain-

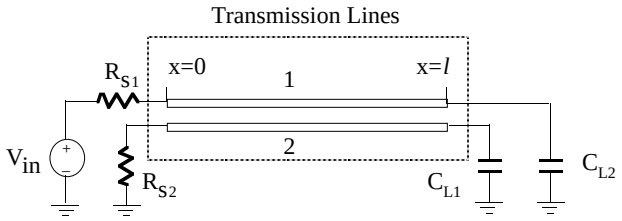

Figure 4.13: Example circuit configuration of coupled lossy transmission lines.

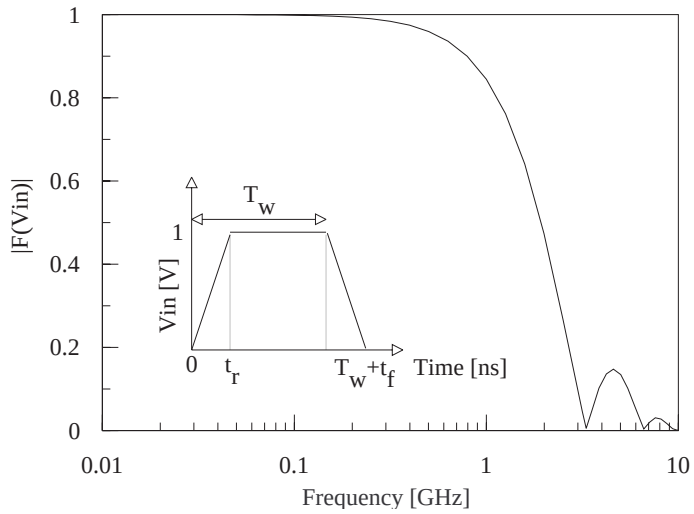

Figure 4.14: Frequency spectra of input pulse, where $t_r = t_f$ = 0.1 ns and T_w = 0.3 ns, producing an effective bandwidth of 2.26 GHz.

ed under two cases assuming lossless *LC* lines and *RLC* lines with DC resistance for all frequencies. As shown in Fig. 4.15(a) the skin and proximity effects disperse the signal and add rise time and delay. Lossy transmission lines with DC resistance generate more crosstalk than pure *LC* assumption, but the skin and proximity effects reduce it, as shown in Fig. 4.15(b), for matched termination. Figure 4.15(c) and (d) show crosstalk voltage vs. varying length of lines for unmatched and matched series termination. Skin and proximity effects reduce the crosstalk more for unmatched termination than for matched termination. For unmatched termination pure *LC* assumption gives the worst crosstalk and dispersive *RLC* lines lessen the crosstalk by

30% from $R_{dc}LC$ assumption. For matched termination $R_{dc}LC$ assumption gives the worst crosstalk, but the difference from the result of dispersive RLC lines is 20% or less, which is not so much as in the case of unmatched termination.

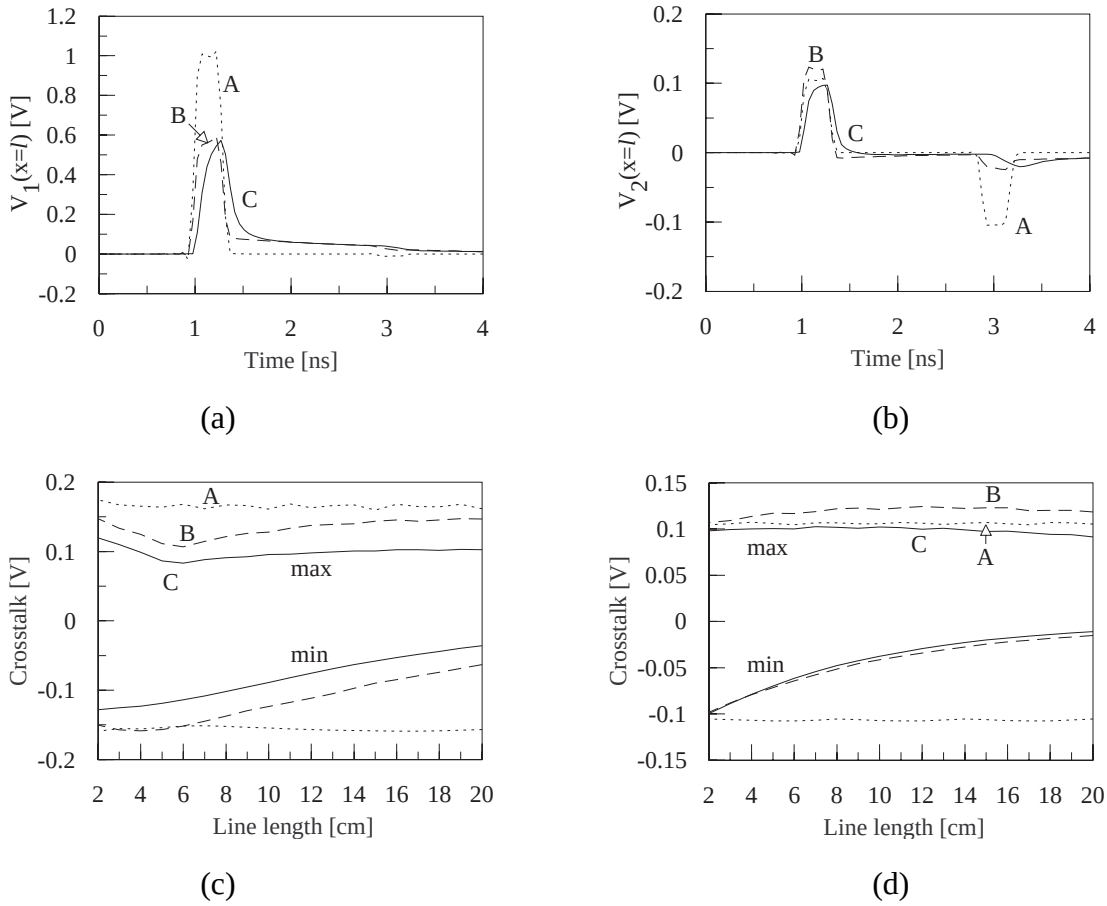

Figure 4.15: Output voltage at the end of the active line and far end crosstalk of the quiet line. (a) Output voltage of the active line with 15 cm length and matched termination, (b) Far end crosstalk of the quiet line with 15 cm length and matched termination, (c) Far end crosstalk vs. line length with unmatched termination, (d) Far end crosstalk vs. line length with matched termination. A(dotted line): pure LC assumption, B(dashed line): $R_{dc}LC$ assumption with DC resistance, C(solid line): RLC lines considering the skin and proximity effects.

4.4 Discussion and Further Considerations

The SRM exploiting the EII has been shown to be accurate and numerically efficient with several examples in calculating frequency dependent resistance and inductance for lossy transmission lines. The SRM reduces considerable number of unknowns by replacing discretization inside the conductor by segmentation only on the conductor surface. Non-uniform segmentation is used for both SRM and VFM, and it considerably reduces computational time. But with SRM much faster computation of series impedance is possible without lose in accuracy.

In addition, SRM can exploit the numerically fast iterative matrix solvers in reference [64] and higher order of basis functions in reference [63] as VFM can, and thus these would add the efficiency of SRM. In general the interconnect structures consist of straight lines which are sequentially connected in series or parallel, and two dimensional approximations for each section gives sufficient information for further stages of circuit simulation. But three dimensional analysis is inevitable for complicated structures in small volumes such as meandering lines, vias, a ground plane with several ports, etc. In following chapter the extension of SRM to three dimensional problems is discussed.